ATIC 310913

NACA

CASE FILE COPY

RESEARCH MEMORANDUM

INVESTIGATION OF A 0.6 HUB-TIP RADIUS-RATIO TRANSONIC

TURBINE DESIGNED FOR SECONDARY-FLOW STUDY

I - DESIGN AND EXPERIMENTAL PERFORMANCE OF

STANDARD TURBINE

By Harold E. Rohlik, William T. Wintucky, and Herbert W. Scibbe

Lewis Flight Propulsion Laboratory
Cleveland, Ohio

CLASSIFICATION CHANGED TO
DECLASSIFIED AUTHORITY

6653   4/23/61

NATIONAL ADVISORY COMMITTEE
FOR AERONAUTICS

WASHINGTON
January 9, 1957

DECLASSIFIED

NATIONAL ADVISORY COMMITTEE FOR AERONAUTICS

RESEARCH MEMORANDUM

INVESTIGATION OF A 0.6 HUB-TIP RADIUS-RATIO TRANSONIC TURBINE

DESIGNED FOR SECONDARY-FLOW STUDY

I - DESIGN AND EXPERIMENTAL PERFORMANCE OF STANDARD TURBINE

By Harold E. Rohlik, William T. Wintucky, and Herbert W. Scibbe

SUMMARY

A transonic turbine with a 0.6 hub-tip radius ratio was designed and built in order to investigate the effect of stator and rotor secondary flows on turbine performance. The experimental performance and results of detailed stator and rotor exit surveys of the standard turbine are presented herein.

Turbine efficiency based on total pressure at design equivalent speed and specific work was 0.863, while rating efficiency was 0.855, indicating an exit whirl loss of 0.008. The maximum value of total efficiency was 0.886 and occurred near 120 percent design speed at 90 percent of design work. Stator exit surveys indicated a total-pressure loss of 0.025 with little radial flow from outer to inner wall. Rotor exit surveys showed lowest values of local efficiency occurring at the inner and outer walls and near the blade midspan. This loss pattern is believed to result from secondary flows in the rotor-blade pressure-surface boundary layers.

INTRODUCTION

Secondary-flow phenomena occurring in turbine stators and in a low-speed turbine have been investigated at the NACA Lewis laboratory and are reported in references 1 to 3. These investigations were concerned with the magnitudes and directions of secondary flows which resulted in accumulations of low-velocity air near the blade ends. The effect of these loss accumulations on turbine performance is considered in reference 4, which includes a study of turbine rotor exit surveys; this report shows that local efficiency in the exit annulus varied as much as 14 percent. These variations were clearly related to stator losses in that the loss patterns were repeated at distances approximately equal to the stator-blade spacing.

In order to investigate the effect of stator and rotor secondary flows on the over-all turbine performance in the transonic range of internal-flow velocities, the turbine described in this report was designed and built. Design parameters for this turbine were selected with a secondary purpose in view. This purpose was to extend the knowledge of the over-all performance as well as of the internal aerodynamics of transonic turbines. This turbine differs from other transonic turbines in that it has a lower hub-tip radius ratio. Information obtained in this investigation is compared with previous work on transonic turbines.

The purpose of this report is to present design information, over-all performance, and results of detailed surveys of flow made at the exit of both blade rows at design equivalent blade speed and equivalent specific work. Over-all performance is presented for a pressure-ratio range of 1.4 to that corresponding to limiting-loading. Survey results are shown in terms of stator total-pressure ratio, local efficiency at the rotor exit, and basic boundary-layer parameters. Over-all performance and survey information obtained from this configuration will be used as a standard for comparison with subsequent results obtained from the same turbine modified to alter secondary-flow characteristics.

SYMBOLS

The following symbols are used in this report:

A flow area, sq ft

D diffusion parameter

g acceleration due to gravity, 32.17 ft/sec^2

Δh specific enthalpy drop, Btu/lb

l mean camber length, ft

N rotative speed, rpm

p absolute pressure, lb/sq ft

R gas constant, ft-lb/(lb)($^{\circ}$R)

r radius, ft

T total temperature, $^{\circ}$R

U blade velocity, ft/sec

CONFIDENTIAL   3

V   absolute gas velocity, ft/sec

W   relative gas velocity, ft/sec

w   weight flow, lb/sec

α   absolute gas flow angle measured from axial direction, deg

γ   ratio of specific heats

δ   ratio of inlet-air total pressure to NACA standard sea-level
        pressure

ε   function of γ, $\dfrac{\gamma_{sl}}{\gamma}\left[\dfrac{\left(\dfrac{\gamma+1}{2}\right)^{\frac{\gamma}{\gamma-1}}}{\left(\dfrac{\gamma_{sl}+1}{2}\right)^{\frac{\gamma_{sl}}{\gamma_{sl}-1}}}\right]$

η   adiabatic efficiency, ratio of turbine work based on torque, weight
        flow, and speed measurements to ideal work based on inlet total
        temperature, and inlet and outlet total pressure, both defined
        as sum of static pressure plus pressure corresponding to gas
        velocity

η_x adiabatic efficiency, ratio of turbine work based on torque, weight
        flow, and speed measurements to ideal work based on inlet total
        temperature, and inlet and outlet total pressure, both defined as
        sum of static pressure plus pressure corresponding to axial
        component of velocity

θ_{cr} squared ratio of critical velocity at turbine inlet to critical
        velocity at NACA standard sea-level temperature, $V_{cr}/V_{cr,sl}$

θ^* momentum-loss parameter

$\bar{\theta}$ effective rotor-blade momentum thickness, ft

ρ   gas density, lb/cu ft

Subscripts:

an   annulus area

4

CONFIDENTIAL

NACA RM E56J16

cr   conditions at Mach number of 1.0

fs   free stream

m   mean radius

s𝑙   NACA standard sea-level conditions

t   tip

tot   sum of suction- and pressure-surface quantities

u   tangential direction

x   axial direction

0   station upstream of stator

1   station at throat of stator passage

2   station at outlet of stator just upstream of trailing edge

3   station at free-stream condition between stator and rotor

4   station at throat of rotor passage

5   station at outlet of rotor just upstream of trailing edge

6   station downstream of turbine

7   station 4 ft downstream of rotor

Superscripts:

'   absolute total state

"   total state relative to rotor

TURBINE DESIGN

Design Requirements

The turbine investigated had a 16-inch tip diameter and a 0.6 hub-tip radius ratio. Design conditions were selected to provide hub relative Mach numbers of 1.0 at the inlet as well as the exit of the rotor.

CONFIDENTIAL

Design-point parameters chosen to meet these conditions are:

$\dfrac{\Delta h'}{\theta_{cr}}$, Btu/lb 21.70

$\dfrac{w\sqrt{\theta_{cr}}}{\delta}\ \epsilon$, lb/sec 21.17

$\dfrac{U_t}{\sqrt{\theta_{cr}}}$, ft/sec 696

Velocity Diagrams

Design velocity diagrams were calculated for stations 0, 2, 3, 5, and 6 and are presented in figure 1. The following assumptions were used to obtain the diagrams:

(1) Free-vortex flow and simplified radial equilibrium at stations 3 and 6

(2) Total-pressure ratio p_3'/p_0' of 0.97 across the stator

(3) Turbine efficiency of 0.88 based on exit total pressure

The design velocity diagrams at station 2 were obtained with the following equations and known conditions at station 3:

$$\left(\frac{V_u}{V_{cr}}\right)_2 = \left(\frac{V_u}{V_{cr}}\right)_3 \tag{1}$$

$$p_2' = p_3' \tag{2}$$

$$\left(\frac{\rho V_x}{\rho' V_{cr}}\right)_2 = \left(\frac{\rho V_x}{\rho' V_{cr}}\right)_3 \frac{A_{3,an}}{A_2} \tag{3}$$

Station 5 diagrams were obtained similarly using station 6 conditions and the following equations:

$$\left(\frac{W_u}{W_{cr}}\right)_5 = \left(\frac{W_u}{W_{cr}}\right)_6 \tag{4}$$

$$p_5'' = p_6'' \tag{5}$$

$$\left(\frac{\rho W_x}{\rho'' W_{cr}}\right)_5 = \left(\frac{\rho W_x}{\rho'' W_{cr}}\right)_6 \frac{A_{6,an}}{A_5} \tag{6}$$

The design exit flow angle α_6 is -5.1^O at the mean section. The energy associated with the exit whirl results in a difference of 0.003 between rating and total efficiency.

At design operation of the turbine, the theoretical margin between design work and limiting work at design speed is only 0.24 Btu per pound, or 1.1 percent of design work. This figure was estimated by using the theoretical curve of limiting tangential velocity based on two-dimensional flow as shown in reference 5.

Stator Design

The turbine stator blades were designed with straight portions downstream of the throats and thin trailing edges in order to get a low level of loss and to minimize the accumulations of low-velocity air. The blades were highly loaded, however, with some suction-surface diffusion. The blades were laid out in the manner described in reference 6, and surface velocities were calculated using the three-dimensional channel analysis described in reference 6 and modified in reference 7.

Blade profiles and channels are shown in figure 2. Blade surface and midchannel velocity distributions are shown in figure 3(a) for the area between the first and last orthogonals calculated. Table I shows blade coordinates and leading- and trailing-edge radii. Stator-blade solidity varied from 2.28 at the hub to 1.46 at the tip. Figure 4 is a photograph of the stator assembly.

Rotor Design

The turbine rotor was designed for 23 blades. This number resulted from the arbitrary specification of a suction-surface diffusion limit of 0.10 and an axial chord of 3.2 inches. The resulting rotor-blade solidities selected to satisfy the design requirements were 2.07 and 1.58 at hub and tip, respectively. The resulting average diffusion on the suction surface was 0.058, where this average was obtained by applying Simpson's rule to a curve through the hub, mean, and tip values plotted against radius. The average pressure-surface diffusion obtained in the same manner was 0.506, giving a total diffusion of 0.564. Blade surface velocities were calculated in the same manner as those of the stator except that relative conditions were used. The calculated velocities are shown in figure 3(b) for the surfaces between the first and last orthogonals calculated. The suction surfaces were designed with straight

sections at the inlet and outlet. Blade profiles are shown in figure 2. Coordinates and setting angle are shown in table II. Figure 5 is a· photograph of the turbine rotor.

APPARATUS

The components of the cold-air test facility, shown in figure 6, consisted primarily of inlet piping for combustion air supply, filter and inlet tanks, turbine test section, discharge collector and piping, and an eddy-current dynamometer. Dry combustion air was admitted through a thin-plate orifice in the inlet piping and entered the turbine test section after passing through the filter and inlet tanks. Immediately downstream of the test section, the airflow was directed through the discharge housing and collector into the laboratory altitude exhaust system. The power output of the turbine was absorbed by a cradled eddy-current dynamometer directly coupled to the turbine rotor shaft.

The 21 steel stator blades were fastened in steel rings at the hub and tip radii. The thin trailing edges of the blades were supported at the tip to minimize vibration caused by the high air velocities. The 23 rotor blades were machined from an aluminum alloy, with a radial clearance of 0.030 inch between the rotor-blade tips and the turbine casing. Axial clearance between the stator and rotor blades was about 1.4 inches at the· mean section. This clearance was dictated by the mechanical design of the survey equipment and the stator assembly. The flanges supporting the stator assembly were complicated by the inclusion of a chamber over the blade tips to provide for possible boundary-layer air bleed in future investigations.

INSTRUMENTATION

Over-All Performance

The airflow measurements were made with a standard submerged thin-plate orifice with sufficiently long straight sections of pipe on either side. The orifice was calibrated after installation.

The torque output of the turbine was measured with an air-balancing thrust-torque cell connected to a mercury column. The torque cell was calibrated for every performance test run. Turbine speed was measured by an electronic events-per-unit-time meter. The inlet temperature was obtained by averaging the readings from two shielded total-temperature thermocouples located in the same plane as the inlet pressure probe and spaced 180° apart.

The turbine-outlet static pressures on the inner and outer annulus walls were obtained by averaging the readings from four taps spaced 90° apart on each of the walls (station 6, fig. 6). In the same plane, absolute flow angles were measured in a radial traverse using an X-Y recorder electronically coupled to a self-alining actuator containing a miniature total-pressure and angle probe. The outlet total temperature was obtained by averaging the readings from four probes spaced 90° apart, each containing five spike thermocouples (station 7, fig. 6).

All pressure measurements were made using mercury manometers with the exception of the pressure difference across the inlet weight flow orifice, for which an acetylene tetrabromide manometer was used. Calibrated iron-constantan thermocouples in conjunction with a spotlight galvanometer and potentiometer were used in measuring all temperatures. The velocity level past the thermocouples was in the low subsonic region; so it was unnecessary to apply a recovery factor to the temperature readings.

Detailed Surveys

Detailed total-pressure surveys were made downstream of the stator at station 3 (fig. 6) with a combination total-pressure and angle probe secured in a self-alining actuator. Total-pressure - flow variations obtained by circumferential travel of the probe at various radii were transmitted by a strain-gage pressure transducer to an X-Y recorder. The circumferential pressure trace measures the difference between the inlet total pressure at station 0 and the total pressure at the survey probe.

A single circumferential traverse was made with a pressure probe which sensed total pressure approximately 0.005 inch downstream of the trailing edge. This probe was mounted in the same actuator, set at the blade exit angle, and operated with a pressure transducer and an X-Y recorder.

At station 6 downstream of the rotor, total pressure, angle, and temperature were recorded in the same manner as at station 3. The spike thermocouple on a combination total-pressure - flow-angle - total-temperature probe, calibrated for recovery, measured the temperature differential from the inlet total-temperature probes at station 0. Circumferential pressure variations were referenced against a static pressure at station 3.

EXPERIMENTAL PROCEDURE

Over-All Performance

The turbine was operated at a constant nominal inlet pressure of 40 inches of mercury absolute and a temperature of 80° F for a range of total-pressure ratios from 1.4 to a value corresponding to limiting-loading of the rotor blades. For each total-pressure ratio investigated, the speed was varied from 40 to 120 percent of the design value in even increments of 10 percent.

A radial survey of flow angle was made downstream of the rotor (station 6) for each data point investigated.

Stator Surveys

Annular surveys of total pressure and flow angle were made in a radial plane approximately 0.8 inch downstream of the stator-blade trailing edges at the mean radius. The area covered by the surveys was a 45° sector of the stator exit annulus, approximately 2.6 stator passages.

Average static pressure at the stator exit was set at the design value, and surveys were made without the rotor in place.

Rotor Surveys

Rotor exit surveys of total pressure, flow angle, and total temperature were made at design equivalent blade speed and equivalent specific work approximately 1 chord length downstream of the rotor trailing edge. These surveys also covered a 45° sector of the exit annulus.

CALCULATIONS

The turbine performance map shown in figure 7(a) shows contours of turbine total-pressure ratio based on total pressure at the turbine exit. The map in figure 7(b), however, shows total-pressure ratio based on the rating or axial component of total pressure at the turbine exit, thus including as a loss the kinetic energy of the exit whirl velocity.

Inlet total pressure was calculated using the following equation, which is a rearranged form of an equation in reference 6, and known values of inlet flow area, inlet total temperature, weight flow, and inlet static pressure:

$$\frac{w\sqrt{T_0'}}{p_0 A_{an,0}} = \left[\frac{2\gamma g}{(\gamma-1)R}\right]^{1/2}\left\{\left[\left(\frac{p'}{p}\right)_0^{\frac{\gamma-1}{\gamma}} - 1\right] + \left[\left(\frac{p'}{p}\right)_0^{\frac{\gamma-1}{\gamma}} - 1\right]^2\right\}^{1/2} \tag{7}$$

Turbine-exit rating pressure was calculated from the following equation using exit annular area and measured values of static pressure, total temperature, weight flow, and flow angle:

$$\frac{w\sqrt{T_7'}}{p_6 A_{an,6}} \cong \left[\frac{2\gamma g}{(\gamma-1)R}\right]^{1/2}\left\{\left[\left(\frac{p_x'}{p}\right)_6^{\frac{\gamma-1}{\gamma}} - 1\right] + \left[\frac{\left(\frac{p_x'}{p}\right)_6^{\frac{\gamma-1}{\gamma}} - 1}{\cos\alpha_6}\right]^2\right\}^{1/2} \tag{8}$$

Turbine-exit total pressure was calculated with the same parameters and the following equation:

$$\frac{w\sqrt{T_7'}}{p_6 A_{an,6}\cos\alpha_6} = \left[\frac{2\gamma g}{(\gamma-1)R}\right]^{1/2}\left\{\left[\left(\frac{p'}{p}\right)_6^{\frac{\gamma-1}{\gamma}} - 1\right] + \left[\left(\frac{p'}{p}\right)_6^{\frac{\gamma-1}{\gamma}} - 1\right]^2\right\}^{1/2} \tag{9}$$

Stator-blade momentum-loss parameter θ^* and total-pressure ratio p_3'/p_0' were calculated with the method described in reference 8. Rotor-blade effective-momentum-thickness parameter was obtained with the method of reference 9.

The total diffusion parameter D_{tot} is the sum of the suction- and pressure-surface diffusions.

RESULTS AND DISCUSSION

Over-All Performance

Figure 7 shows turbine equivalent specific work plotted against weight flow - speed parameter with contours of percent equivalent design speed, pressure ratio, and efficiency. The total efficiency at design equivalent blade speed and equivalent specific work was 0.863 (fig. 7(a)). Limiting-loading work at design speed was 21.90 Btu per pound, 0.9 percent above design work. This difference agrees very well with the design figure of 1.1 percent, indicating that both stator- and rotor-blade rows were operating at design exit tangential velocities. Figure 7(b) shows a design-point rating efficiency of 0.855, 0.008 less than the total efficiency. This exit whirl loss is slightly greater than the design figure of 0.003.

The highest total efficiency, 0.886, occurred near 120 percent design speed and about 90 percent design work.

Stator Exit Surveys

Contours of stator total-pressure ratio (fig. 8) show loss accumulations at both blade ends. The accumulation at the hub is only slightly larger, with about the same magnitude of losses, which may be expected from the difference in velocity levels. The similarity of loss accumulations at the blade ends indicates that radial transport of loss material from outer to inner walls is relatively small. This is in contrast with the performance of the stator blades of reference 1, which showed appreciable inward radial flow of low-velocity air in the blade wakes and boundary layers at similar velocity levels. The reason for the apparently small radial flow in the stator-blade row of this investigation is believed to be the reduced flow path resulting from very thin trailing edges, which were approximately one-fourth as thick as those of reference 1.

Radial distribution of momentum loss across the stator-blade row is shown in figure 9 in terms of the momentum-loss parameter θ^*. An additional point was obtained from a mean-section survey which was taken about 0.005 inch downstream of the trailing edge. This survey served as a check on the validity of the annular surveys made in the station 3 survey plane, showing almost exact agreement.

The total-pressure ratio across the stator was 0.975 based on stator exit surveys, static tap readings, and calculated inlet total pressure. This value is shown in figure 10 with values from stators of reference 10 plotted as a function of exit critical velocity ratio at the mean radius. Also shown is the value obtained from a single mean-section survey at the trailing edge in the manner described in reference 10. This method projects the pressure loss in the blade boundary layers at the mean section to the boundary layers of the entire blade and the passage end walls in computing an over-all total-pressure loss. The two values for this stator are in almost exact agreement, indicating that the mean-section survey is representative of the boundary layers of the whole blade and the end walls. The loss in total pressure across the stator, then, appears to result from two-dimensional boundary-layer growth on the blades and end walls without additional loss from secondary flows and mixing.

Rotor Exit Surveys

Annular surveys of total pressure and temperature were used with turbine-inlet conditions to obtain variations in local efficiency at the rotor exit. Contours of efficiency at this station are shown in figure 11. At some radii, a circumferential gradient exists which may result

from a slight time variation in flow conditions, or a stationary distur-
bance which may result from the presence of the survey instrumentation
slot. The loss distribution, however, shows no pattern which may be
clearly associated with the stator blades. In addition to the wall
boundary layers, a band of low efficiency occurs near the midspan of the
rotor blades with bands of higher efficiency on either side. The apparent
lack of the stator-blade loss pattern indicates that the rotor effects a
redistribution of loss material into circumferential bands. The radial
distribution of efficiency is shown more clearly in figure 12, which is
a plot of circumferentially averaged efficiency across two stator-blade
spacings against radius.

A very similar pattern of efficiency distribution was obtained with
turbine 2 of reference 11 with circumferential bands predominating.
Turbine 2 was designed for large pressure-surface diffusion. The average
for hub, mean, and tip was 0.513. In reference 11 the accumulation of
low-efficiency air in a circumferential band near midspan is attributed
to secondary flows on the rotor-blade pressure surface with low-velocity
air flowing radially inward near the leading edge in response to the radial
pressure gradient and then radially outward near the trailing edge where
centrifugal forces on the boundary layers predominate. The same reasoning
may be applied to the turbine rotor of this report, which has an average
pressure-surface diffusion of 0.506. Here again the diffusion and boundary-
layer thickening near the leading edge could result in an inward radial
flow prior to the outward flow which occurs near the trailing edge where
the radial pressure gradient is small.

A rotor-blade effective momentum thickness was calculated for design
operation with the method of reference 9. The resulting value gives a
ratio of momentum thickness to mean camber length $\bar{\theta}_{tot}/l$ of 0.0153.
Figure 13 shows this point plotted on a reproduction of figure 4 of ref-
erence 9. The other points on the curve were obtained from design-point
performance of six transonic turbines. The momentum loss for this turbine
rotor is comparable in magnitude with those of the reference turbines.

SUMMARY OF RESULTS

The design and experimental performance of a 0.6 hub-tip radius-
ratio transonic turbine designed to investigate secondary flows are
presented herein. Results of this investigation are as follows:

1. Turbine efficiency based on total pressure was 0.863 at design
operation while rating efficiency was 0.855, indicating an exit whirl loss
of 0.008. The maximum value of total efficiency was 0.886 and occurred
near 120 percent design speed at 90 percent of design work. Limiting-
loading specific work at design speed was 0.9 percent above design work.

2. Stator exit surveys indicated a total-pressure loss of 0.025, with loss accumulations occurring at the blade ends and apparently little radial flow.

3. Stator-blade momentum loss calculated with trailing-edge survey agreed almost exactly with that obtained from surveys made in the measuring plane 0.8 inch downstream of the trailing edge. Turbine stator total-pressure ratio calculated from the mean-section trailing-edge survey also checked almost exactly with that obtained from a complete annular survey made in the measuring plane, indicating that the blade boundary layers at midspan are representative of the entire blade and end-wall boundary layers.

4. Rotor exit surveys showed a pattern of local efficiency in which circumferential bands predominate with lowest efficiencies occurring at the walls and near midspan. This pattern is believed to result from secondary flows in the rotor-blade boundary layer which flow radially inward in the pressure-surface boundary layer near the leading edge and then radially outward near the trailing edge.

Lewis Flight Propulsion Laboratory
    National Advisory Committee for Aeronautics
        Cleveland, Ohio, October 19, 1956

REFERENCES

1. Rohlik, Harold E., Kofskey, Milton G., Allen, Hubert W., and Herzig Howard Z.: Secondary Flows and Boundary-Layer Accumulations in Turbine Nozzles. NACA Rep. 1168, 1954. (Supersedes NACA TN's 2871, 2909, and 2989.)

2. Kofskey, Milton G., and Allen, Hubert W.: Smoke Study of Nozzle Secondary Flows in a Low-Speed Turbine. NACA TN 3260, 1954.

3. Allen, Hubert W., and Kofskey, Milton G.: Visualization Study of Secondary Flows in Turbine Rotor Tip Regions. NACA TN 3519, 1955.

4. Whitney, Warren J., Buckner, Howard A., Jr., and Monroe, Daniel E.: Effect of Nozzle Secondary Flows on Turbine Performance as Indicated by Exit Surveys of a Rotor. NACA RM E54B03, 1954.

5. Hauser, Cavour H., and Plohr, Henry W.: Two-Dimensional Cascade Investigation of the Maximum Exit Tangential Velocity Component and Other Flow Conditions at the Exit of Several Turbine-Blade Designs at Supercritical Pressure Ratios. NACA RM E51F12, 1951.

6. Stewart, Warner L., Wong, Robert Y., and Evans, David G.: Design and
      Experimental Investigation of Transonic Turbine with Slight Negative
      Reaction Across Rotor Hub. NACA RM E53L29a, 1954.

7. Miser, James W., Stewart, Warner L., and Monroe, Daniel E.: Effect of
      High Rotor Pressure-Surface Diffusion on Performance of a Transonic
      Turbine. NACA RM E55H29a, 1955.

8. Stewart, Warner L.: Analysis of Two-Dimensional Compressible-Flow
      Loss Characteristics Downstream of Turbomachine Blade Rows in Terms
      of Basic Boundary-Layer Characteristics. NACA TN 3515, 1955.

9. Stewart, Warner L., Whitney, Warren J., and Miser, James W.: Use of
      Effective Momentum Thickness in Describing Turbine Rotor-Blade Losses.
      NACA RM E56B29, 1956.

10. Stewart, Warner L., Whitney, Warren J., and Wong, Robert Y.: Use of
      Mean-Section Boundary-Layer Parameters in Predicting Three-
      Dimensional Turbine Stator Losses. NACA RM E55L12a, 1956.

11. Wong, Robert Y., Miser, James W., and Stewart, Warner L.: Qualitative
      Study of Flow Characteristics Through Single-Stage Turbines as Made
      from Rotor-Exit Surveys. NACA RM E55K21, 1956.

DECLASSIFIED

CONFIDENTIAL

TABLE I. - STATOR-BLADE-SECTION COORDINATES
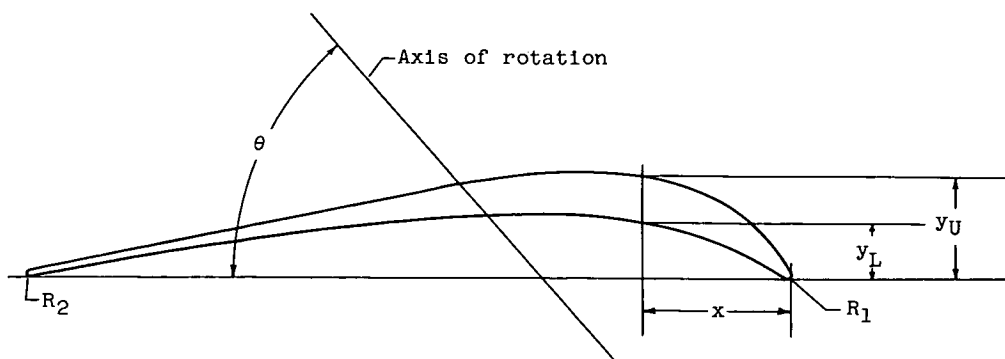
	Section B-B		Section C-C		Section D-D		Section E-E	
θ, deg	52.17		51.50		48.37		43.83	
r/r_t	0.58		0.63		0.83		1.03	
x, in.	y_L, in.	y_U, in.	y_L, in.	y_U, in.	y_L, in.	y_U, in.	y_L, in.	y_U, in.
0	0.015	0.015	0.015	0.015	0.015	0.015	0.015	0.015
.10	.061	.148	.062	.142	.046	.134	.041	.127
.20	.115	.237	.116	.226	.101	.220	.082	.213
.30	.152	.302	.153	.288	.141	.284	.113	.280
.40	.179	.349	.181	.335	.171	.329	.134	.328
.50	.199	.381	.198	.336	.194	.361	.149	.362
.60	.213	.400	.212	.385	.210	.381	.163	.386
.70	.221	.408	.221	.395	.220	.391	.174	.401
.80	.225	.406	.227	.395	.226	.393	.182	.407
.90	.225	.396	.228	.388	.229	.388	.189	.407
1.00	.223	.379	.227	.375	.230	.378	.195	.400
1.10	.219	.357	.224	.358	.229	.364	.199	.389
1.20	.212	.333	.218	.338	.226	.348	.202	.374
1.30	.203	.305	.210	.317	.221	.329	.202	.358
1.40	.192	.276	.201	.294	.215	.310	.201	.340
1.50	.179	.251	.189	.269	.207	.291	.199	.322
1.60	.165	.223	.176	.244	.198	.273	.196	.304
1.70	.150	.196	.162	.218	.188	.253	.192	.287
1.80	.134	.168	.147	.194	.178	.233	.188	.269
1.90	.115	.141	.129	.168	.165	.213	.184	.252
2.00	.093	.114	.111	.144	.152	.193	.177	.235
2.10	.070	.086	.090	.118	.139	.173	.169	.217
2.20	.046	.059	.070	.093	.126	.153	.160	.199
2.30	.020	.032	.049	.067	.111	.134	.151	.181
2.379	.005	.005	----	----	----	----	----	----
2.40	----	----	.027	.040	.096	.115	.139	.163
2.50	----	----	.006	.015	.079	.095	.126	.146
2.537	----	----	.005	.005	----	----	----	----
2.60	----	----	----	----	.061	.076	.112	.127
2.70	----	----	----	----	.043	.057	.096	.108
2.80	----	----	----	----	.023	.037	.079	.090
2.90	----	----	----	----	.004	.017	.061	.072
2.925	----	----	----	----	.005	.005	----	----
3.00	----	----	----	----	----	----	.043	.055
3.10	----	----	----	----	----	----	.024	.036
3.20	----	----	----	----	----	----	.006	.018
3.239	----	----	----	----	----	----	.005	.005
R_1, in.	0.015		0.015		0.015		0.015	
R_2, in.	0.005		0.005		0.005		0.005	

TABLE II. - ROTOR-BLADE-SECTION COORDINATES

Axis of rotation

y_U y_L x R_1 R_2 θ
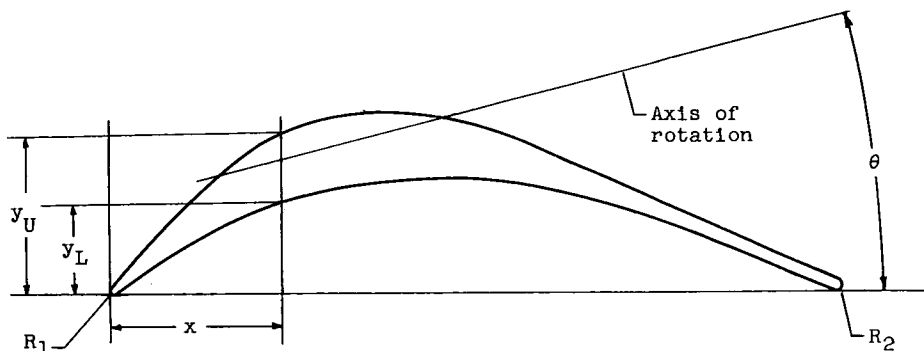
x, in.	Hub		Mean		Tip	
θ, deg	-7.67		13.87		33.47	
r/r$_t$	0.60		0.80		1.00	
	y_L, in.	y_U, in.	y_L, in.	y_U, in.	y_L, in.	y_U, in.
0	0.015	0.015	0.015	0.015	0.015	0.015
.1	.073	.137	.063	.132	.041	.088
.2	.162	.250	.132	.242	.084	.149
.3	.244	.355	.192	.349	.122	.203
.4	.322	.457	.244	.445	.154	.250
.5	.390	.552	.290	.525	.182	.289
.6	.450	.638	.327	.587	.206	.323
.7	.504	.713	.360	.633	.226	.350
.8	.547	.777	.385	.667	.243	.372
.9	.582	.827	.404	.689	.255	.387
1.0	.610	.866	.419	.700	.266	.398
1.1	.632	.892	.429	.700	.273	.404
1.2	.646	.907	.435	.693	.278	.404
1.3	.652	.908	.436	.677	.280	.400
1.4	.650	.899	.433	.653	.280	.393
1.5	.642	.879	.425	.623	.276	.383
1.6	.627	.849	.413	.585	.271	.371
1.7	.602	.806	.399	.543	.264	.356
1.8	.572	.753	.379	.500	.256	.339
1.9	.532	.688	.354	.455	.247	.321
2.0	.487	.615	.326	.411	.236	.302
2.1	.434	.540	.293	.364	.224	.284
2.2	.372	.450	.259	.320	.210	.268
2.3	.305	.367	.223	.276	.196	.250
2.4	.230	.284	.182	.230	.181	.232
2.5	.152	.202	.140	.184	.164	.214
2.6	.070	.119	.096	.140	.148	.196
2.7	----	----	.052	.094	.130	.179
2.710	.019	.019	----	----	----	----
2.8	----	----	.006	.049	.112	.161
2.842	----	----	.019	.019	----	----
2.9	----	----	----	----	.095	.143
3.0	----	----	----	----	.078	.126
3.1	----	----	----	----	.060	.108
3.2	----	----	----	----	.042	.090
3.3	----	----	----	----	.025	.072
3.4	----	----	----	----	.007	.054
3.459	----	----	----	----	.023	.023
R$_1$, in.	0.015		0.015		0.015	
R$_2$, in.	0.019		0.019		0.023	

(a) Hub; r/r_t, 0.60.   (b) Mean; r/r_t, 0.80.   (c) Tip; r/r_t, 1.00.
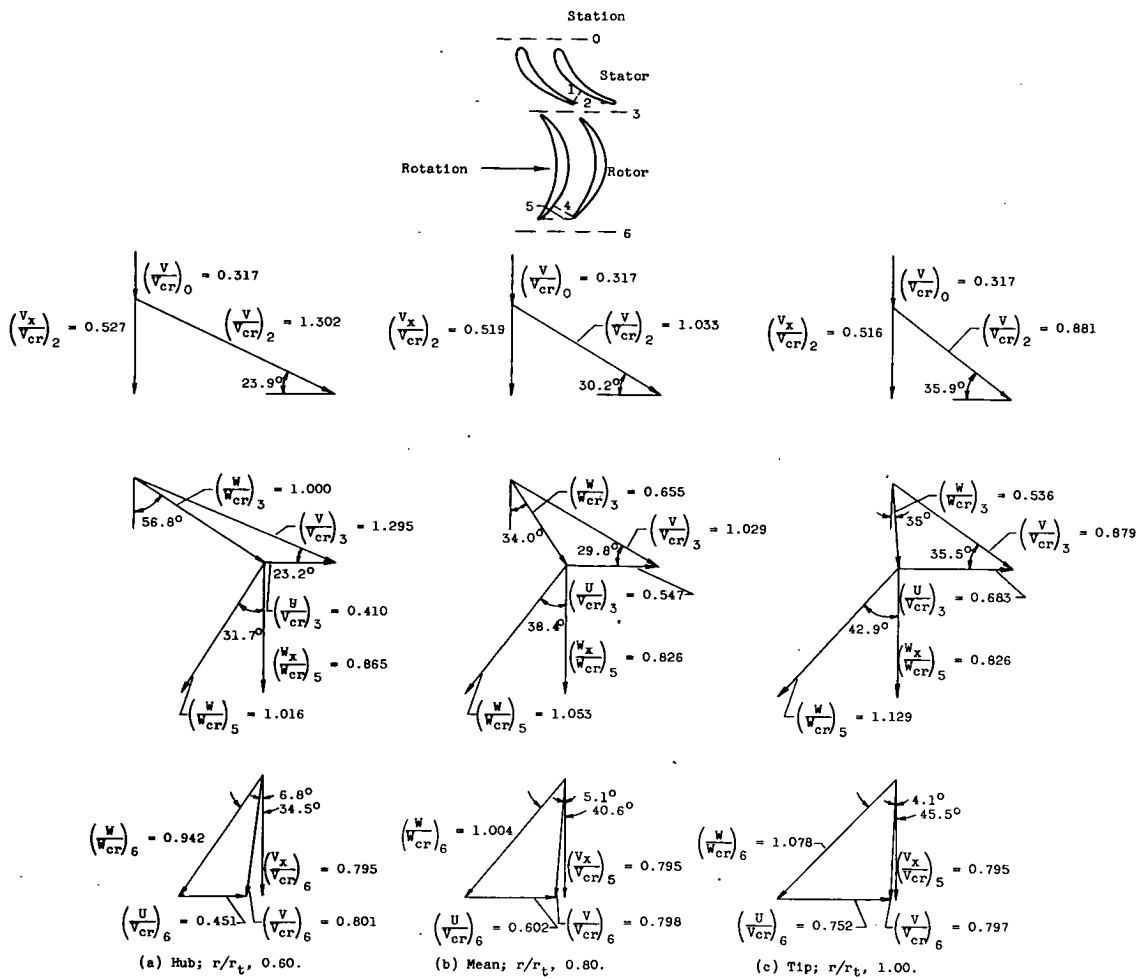
Figure 1. – Design velocity diagrams of transonic secondary-flow turbine.
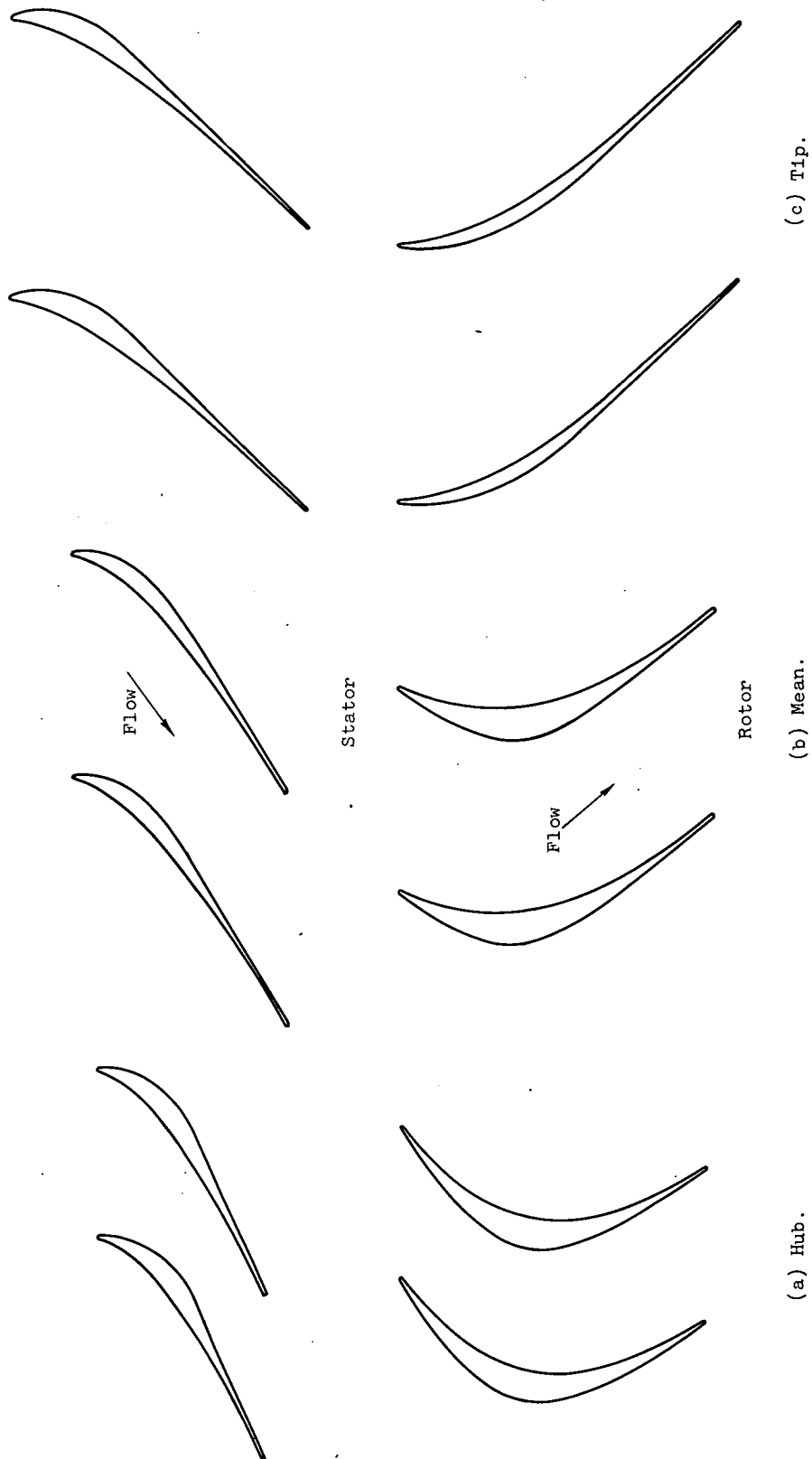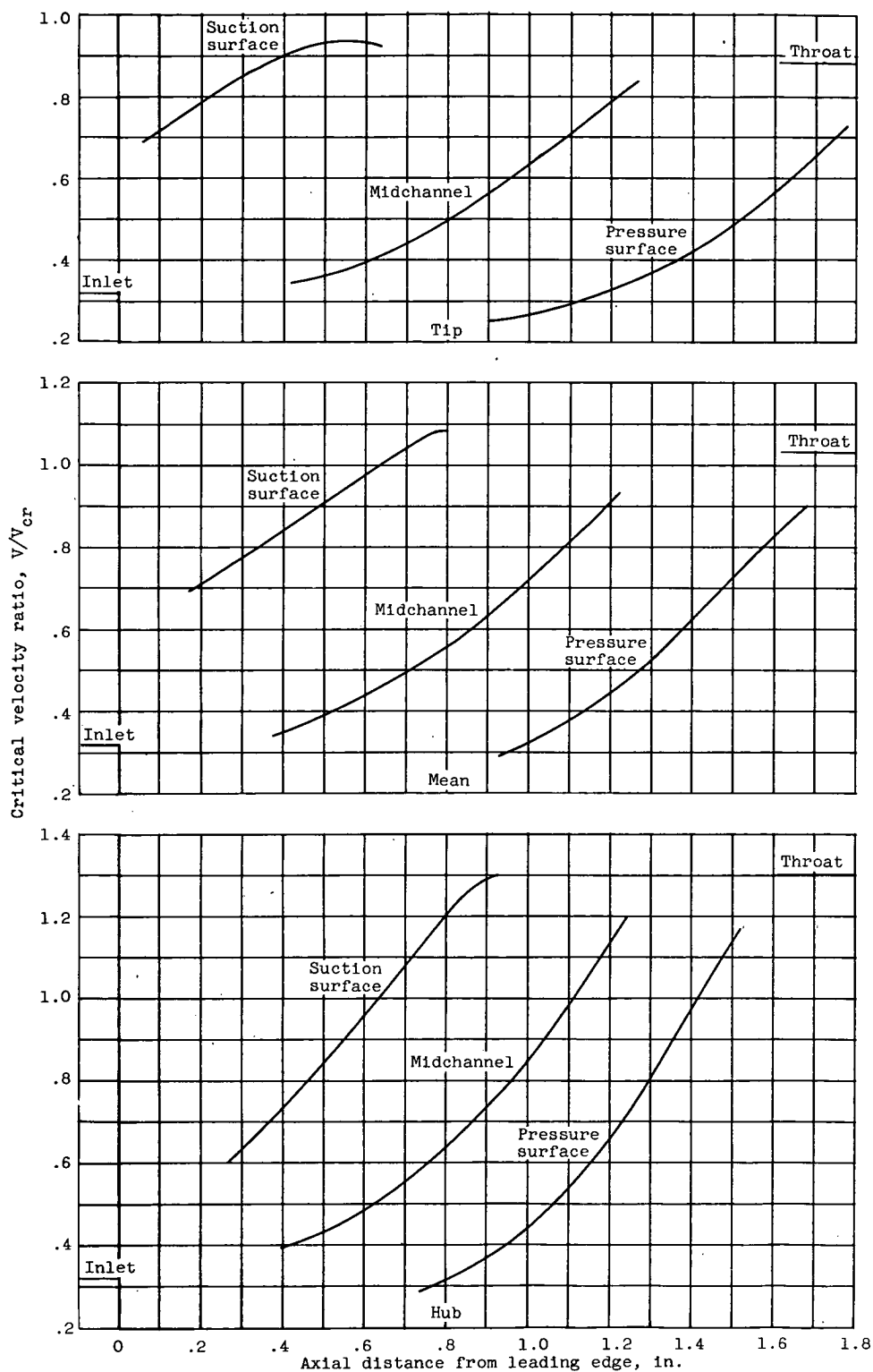
Flow

Stator

Flow

Rotor

(a) Hub.

(b) Mean.

(c) Tip.
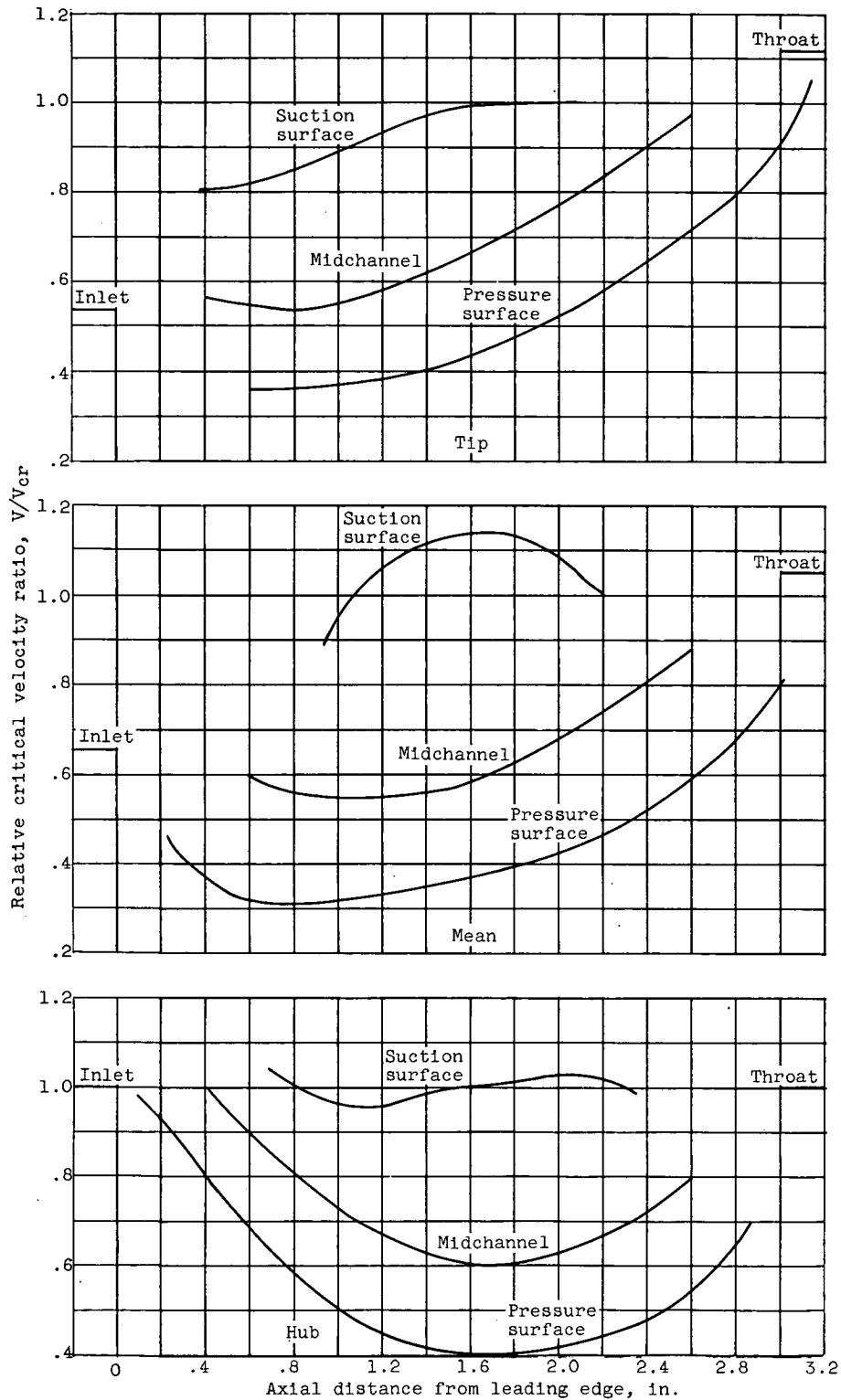
Figure 2. - Blade profiles and channels of transonic secondary-flow turbine.

(a) Stator.

Figure 3. - Calculated blade surface velocities.

(b) Rotor.

Figure 3. - Concluded. Calculated blade surface velocities.
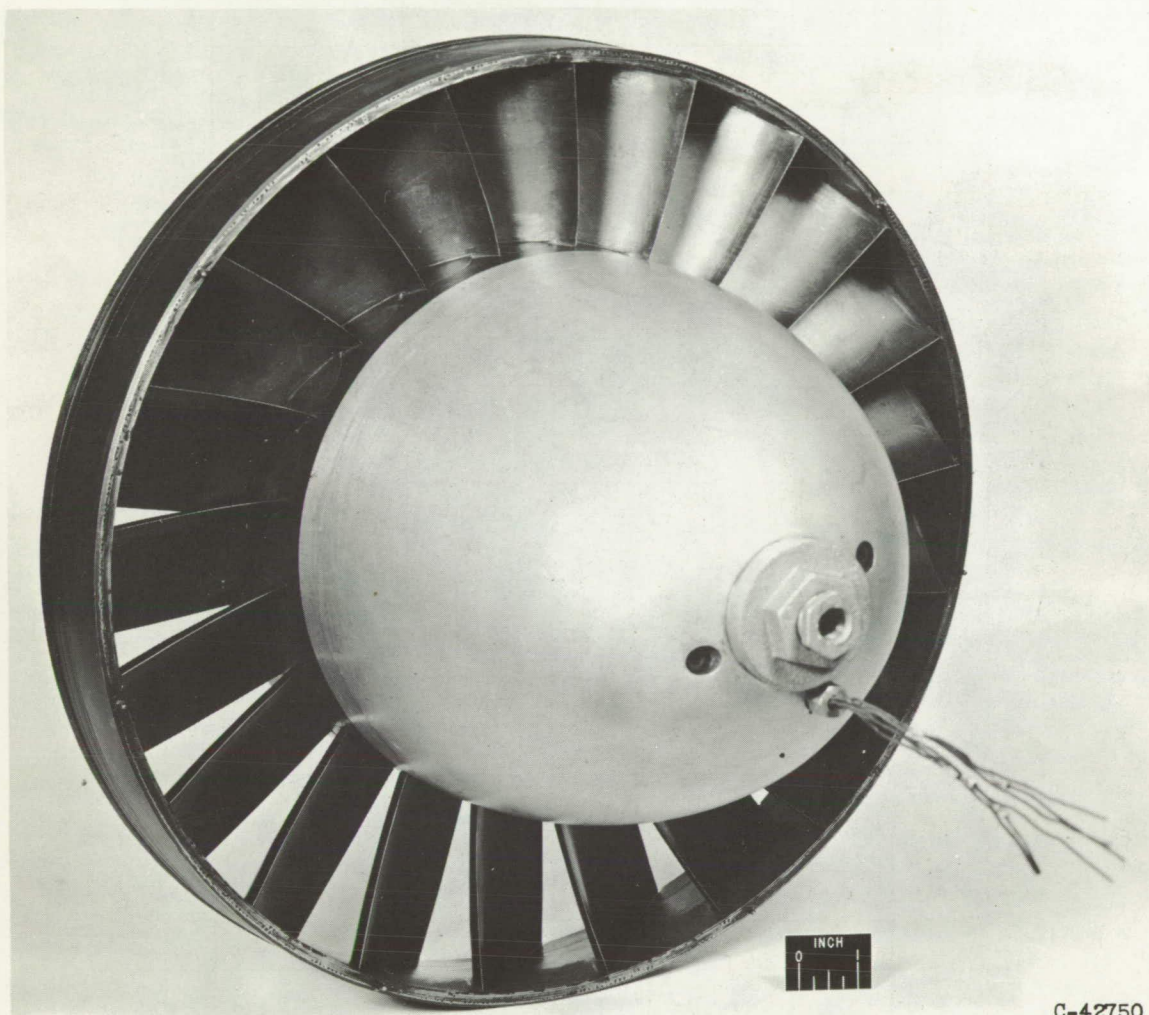
Figure 4. - Turbine standard stator.

C-42750
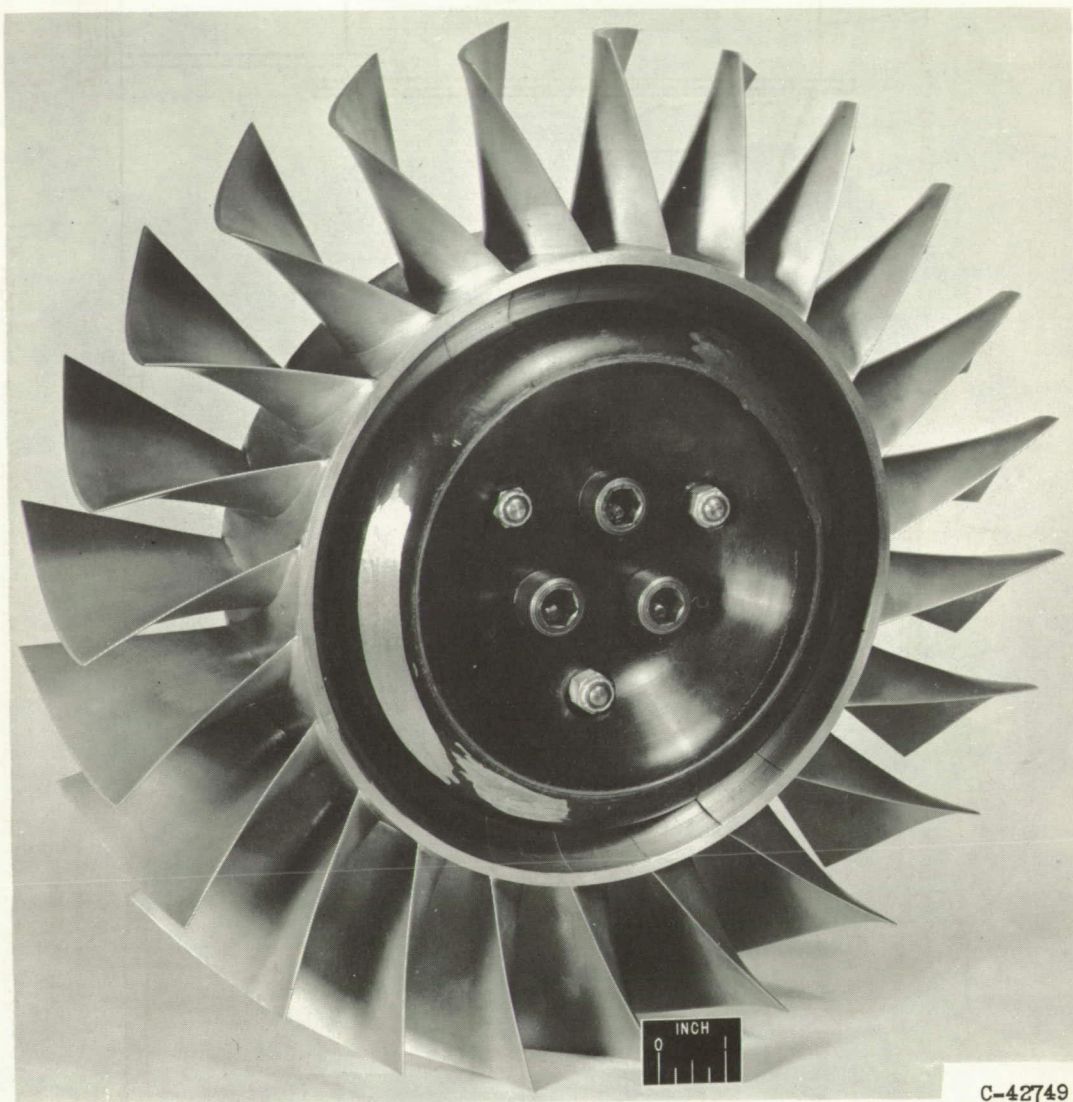
C-42749

Figure 5. - Turbine rotor.
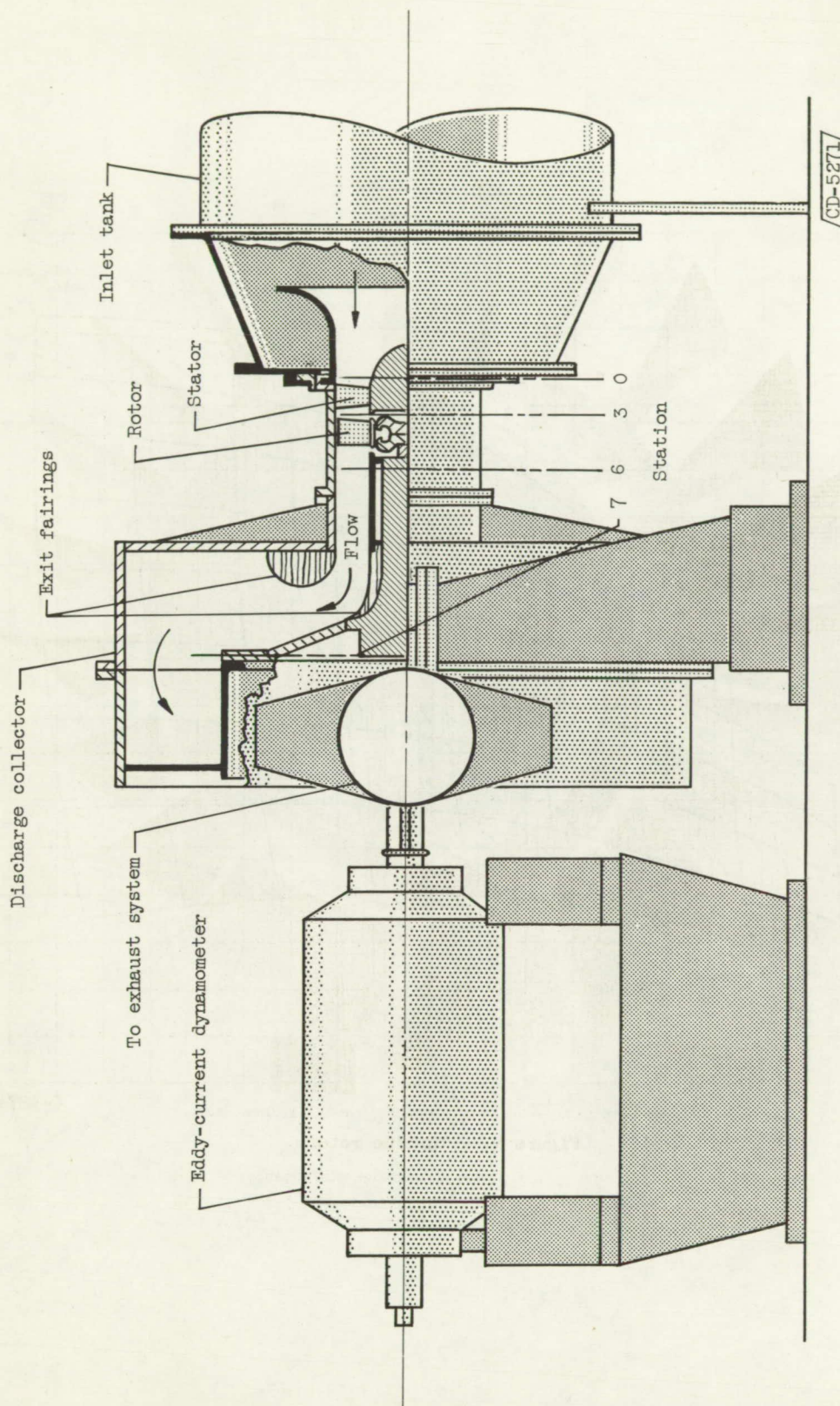
Figure 6. - Diagrammatic sketch of secondary-flow turbine.

⠁⠉⠝⠋⠊⠃⠃⠁⠇⠁⠁⠉
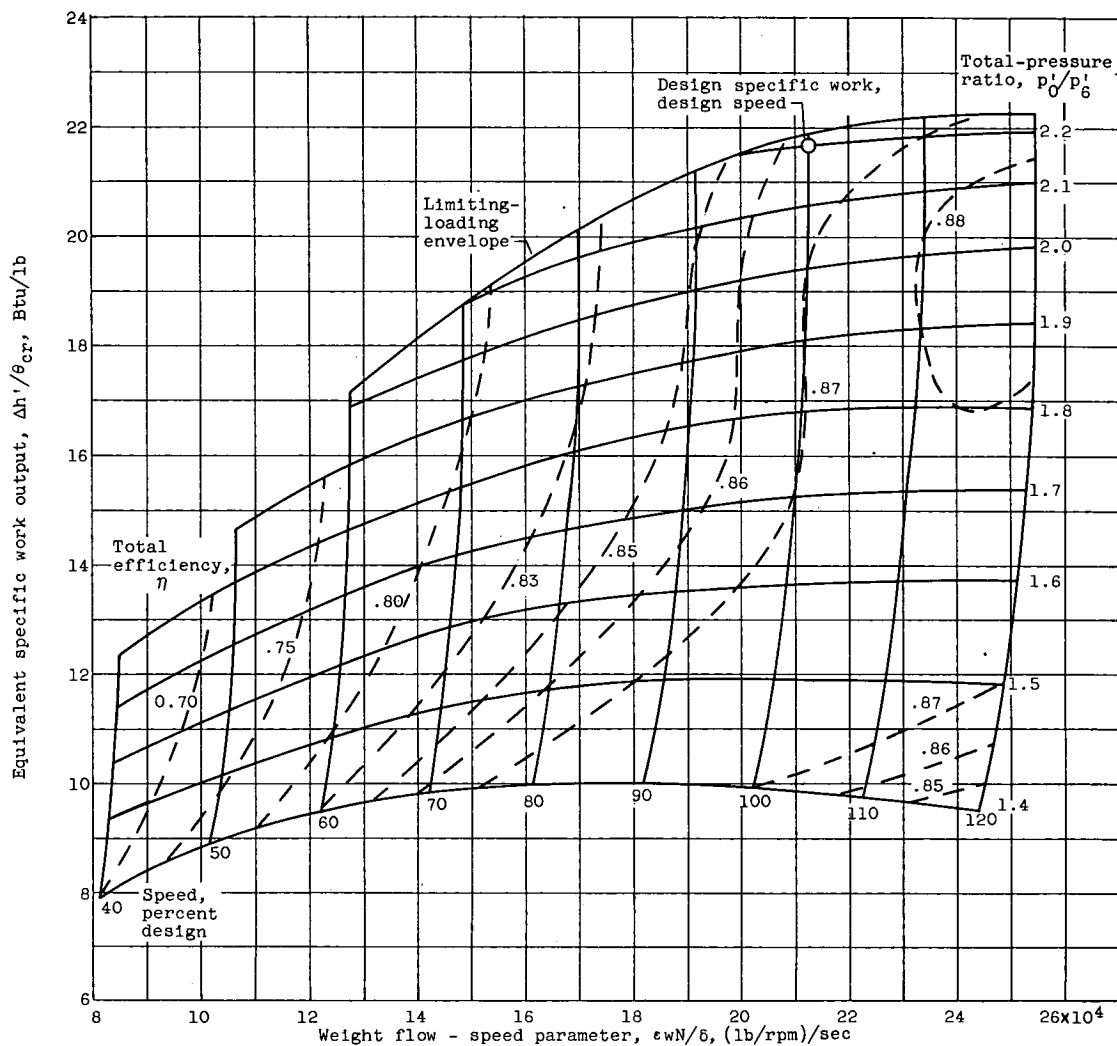
(a) Based on total-pressure ratio.

Figure 7. - Over-all turbine performance.
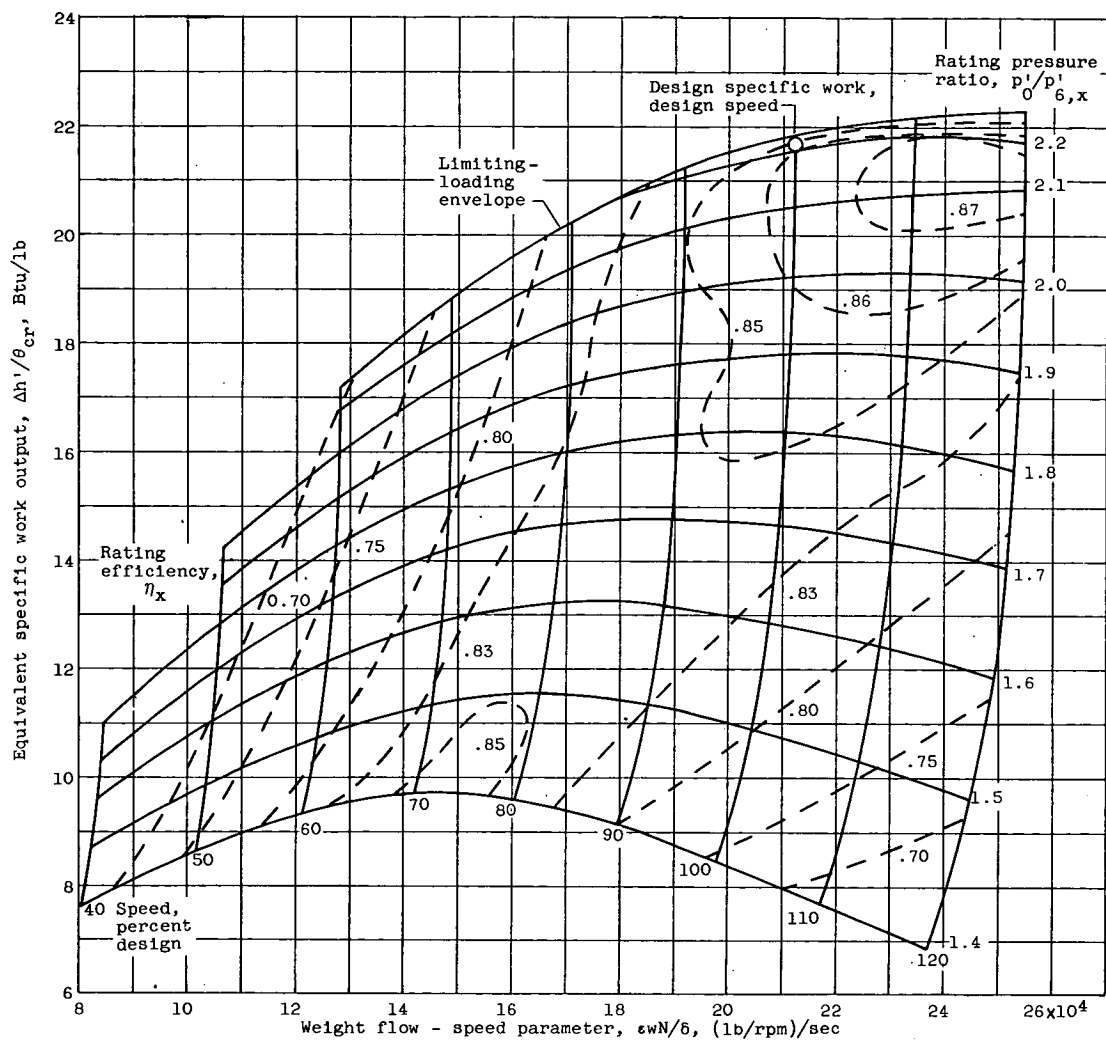
(b) Based on rating pressure ratio.

Figure 7. - Concluded. Over-all turbine performance.

NACA RM E56J16
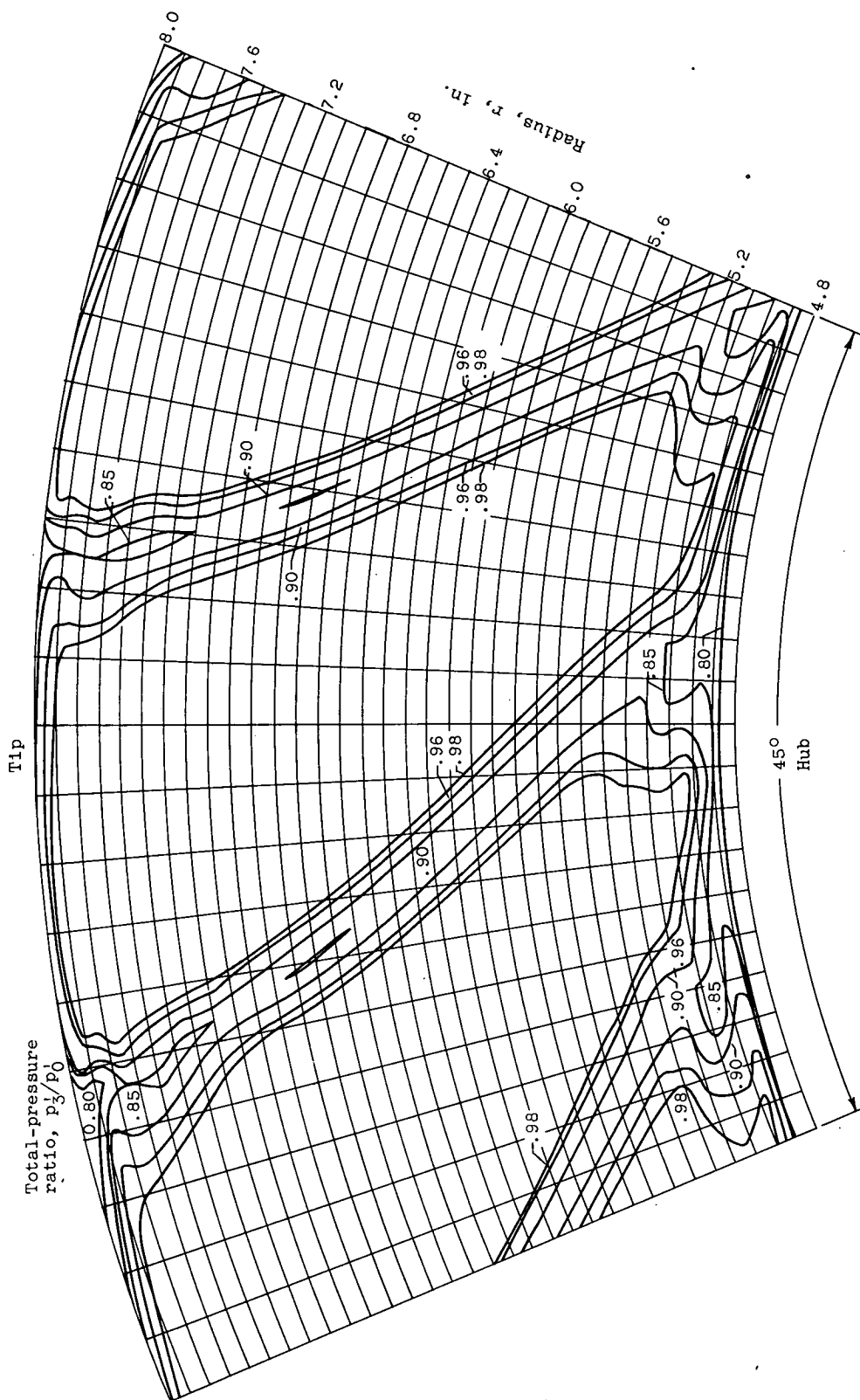
Figure 8. - Contours of total-pressure ratio at stator exit measured at design stator operation.
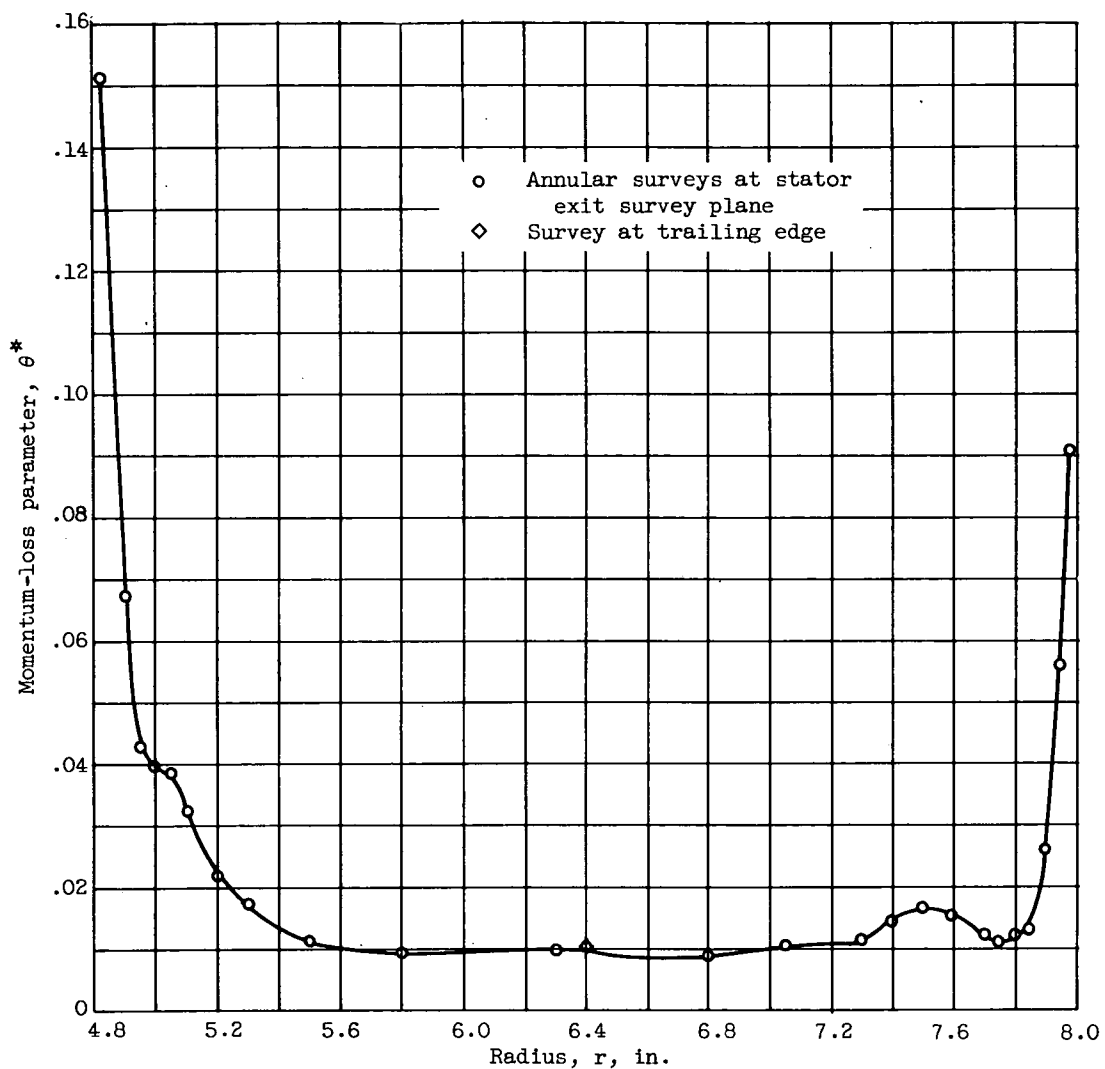
Figure 9. - Radial distribution of momentum-loss parameter at stator exit survey station as determined by surveys made at design stator operation.
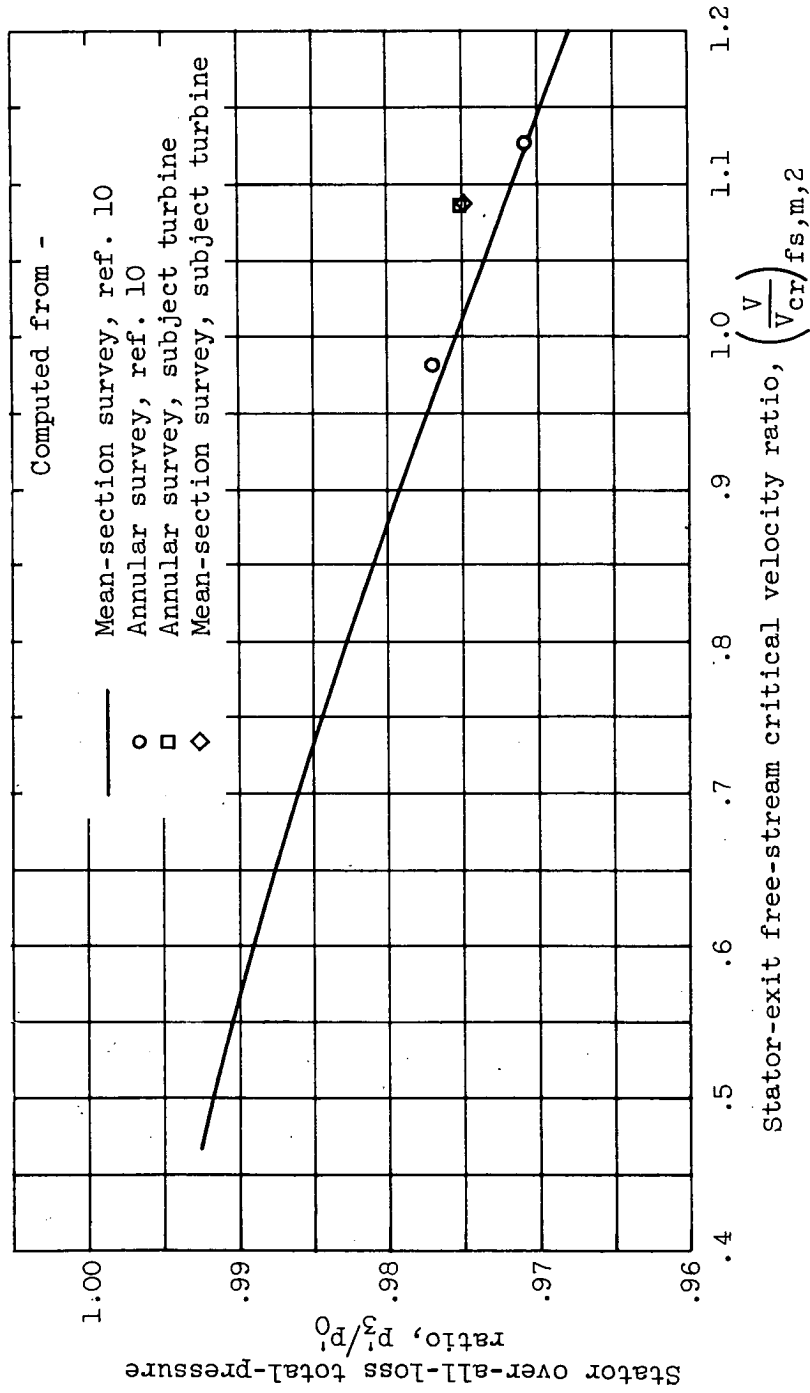
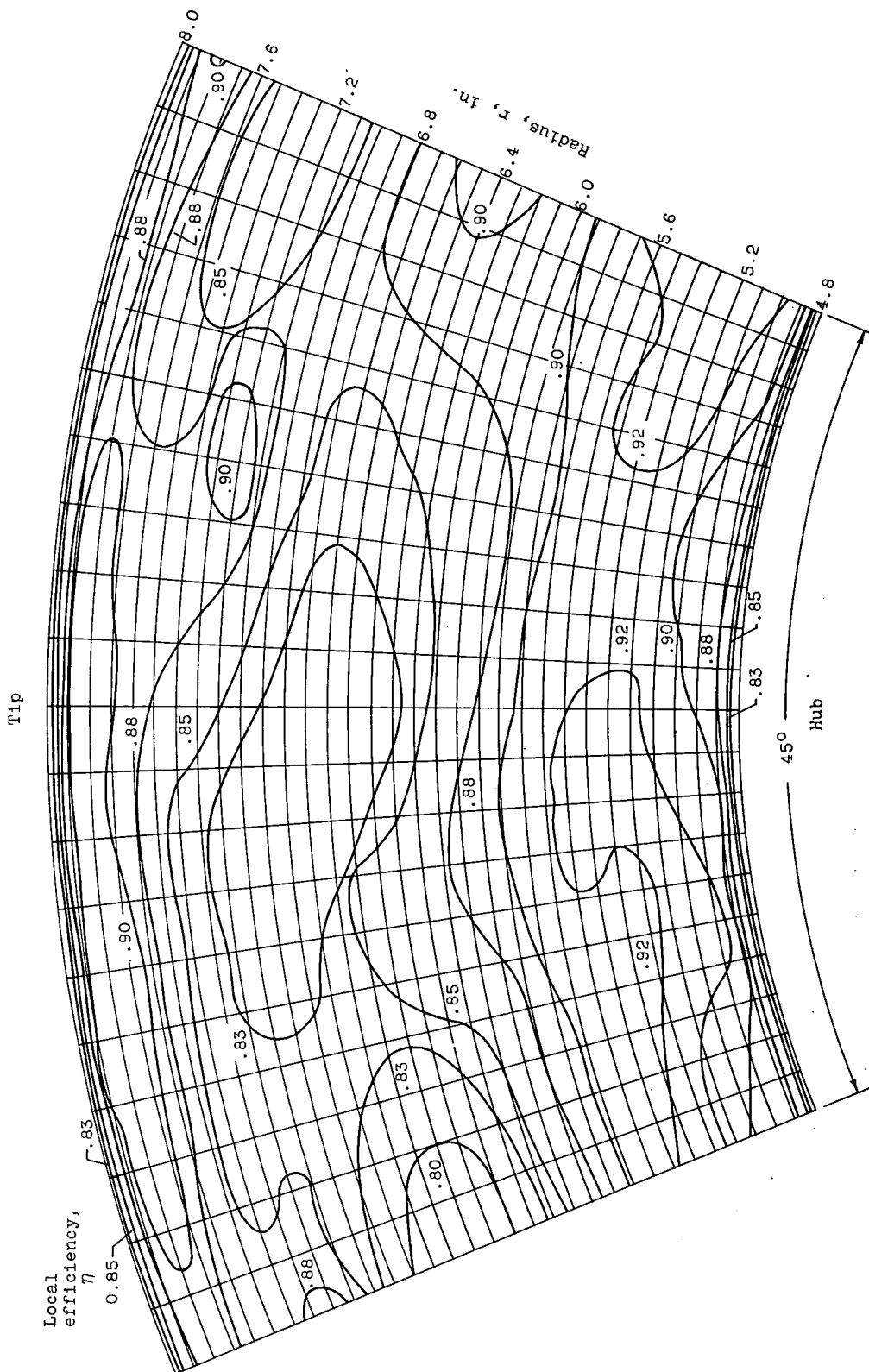Figure 10. - Variation in stator total-pressure ratio with mean-section free-stream critical velocity ratio.

Figure 11. - Contours of local efficiency at rotor exit from surveys made at design operating conditions.

CONFIDENTIAL
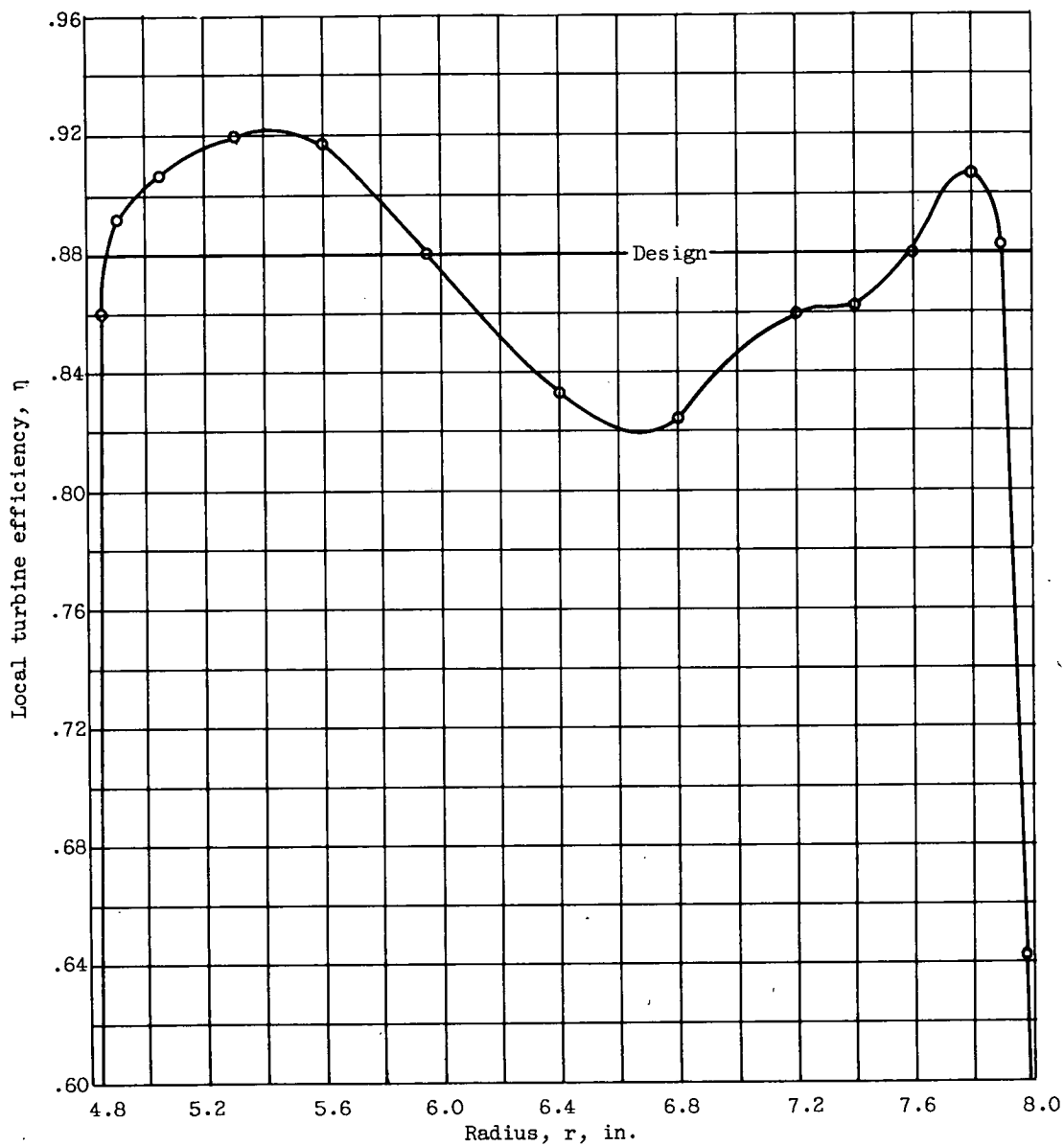
Figure 12. - Radial distribution of circumferentially averaged local efficiency from rotor exit surveys made at design operating conditions.
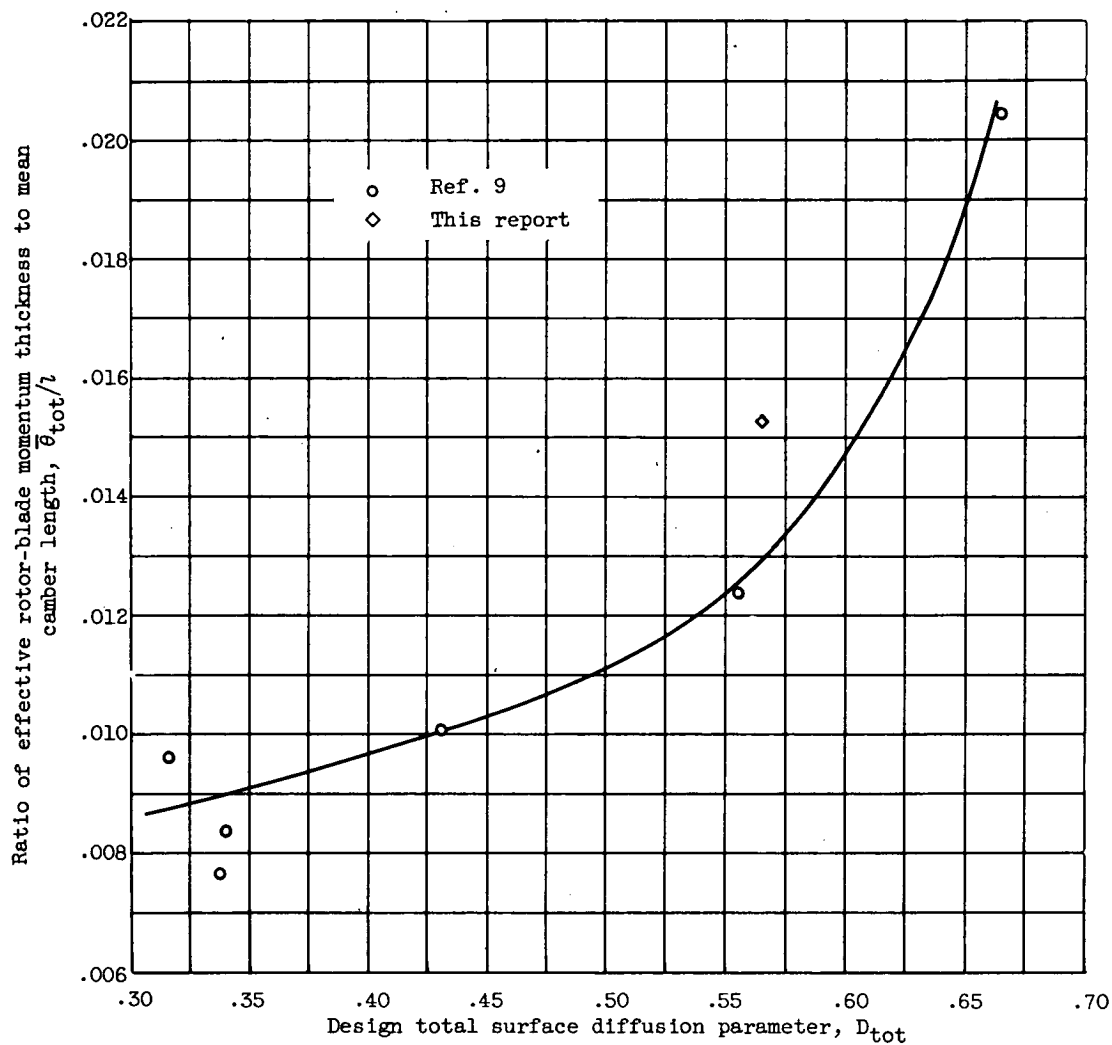
Figure 13. - Variation in ratio of effective rotor-blade momentum thickness to mean camber length with design total surface diffusion parameter.